Spinning Beacons for Precise Indoor Localization

Ho-lin Chang[1] Jr-ben Tian[1] Tsung-Te Lai[1] Hao-Hua Chu[1,2] Polly Huang[2,3]

Department of Computer Science and Information Engineering[1]

Graduate Institute of Networking and Multimedia[2]

Department of Electrical Engineering[3]

National Taiwan University, Taipei, Taiwan

{r95004, r93045, r96152, hchu}@csie.ntu.edu.tw, phuang@cc.ee.ntu.edu.tw

ABSTRACT

This work proposes the novel use of spinning beacons for precise indoor localization. The proposed "SpinLoc" (Spinning Indoor Localization) system uses "spinning" (*i.e.,* rotating) beacons to create and detect predictable and highly distinguishable Doppler signals for sub-meter localization accuracy. The system analyzes Doppler frequency shifts of signals from spinning beacons, which are then used to calculate orientation angles to a target. By obtaining orientation angles from two or more beacons, SpinLoc can precisely locate stationary or slow-moving targets. After designing and implementing the system using MICA2 motes, its performance was tested in an indoor garage environment. The experimental results revealed a median error of 40~50 centimeters and a 90% error of 70~90 centimeters.

Categories and Subject Descriptors

C.2.4 [Computer-Communications Networks]: Distributed Systems

General Terms

Algorithms, Experimentation, Theory

Keywords

Sensor Networks, Spinning Beacons, Doppler Effect, Angulation, Localization

1. INTRODUCTION

Location is often essential contextual information for inferring high-level application semantics from low-level data collected from wireless sensor networks (WSNs) [1][2]. Sensor localization is therefore a critical component in a WSN system. Although GPS is often used for determining position of a sensor node, it performs poorly and inaccurately in indoor environments due to lack of direct line-of-sight to GPS satellites. Consequently, indoor positioning systems using Wi-Fi received signal strength (RSS) and RFIDs have gained popularity. However, despite attempts to improve their positional accuracy, current Wi-Fi RSS and RFID systems are unable to achieve the sub-meter accuracy required for many indoor WSN applications such as personnel tracking in crowded hospitals or asset tracking in busy factories. Thus, high-precision indoor localization remains a challenging research problem.

Current high-precision indoor localization systems with sub-meter accuracy employ varying methods of overcoming indoor multipath interference. For example, the Ubisense [3] system uses ultra-wideband (UWB) to minimize multipath interference. However, UWB-based systems [3][4][5] require specialized hardware to achieve sampling rates and time synchronization in GHz and nanosecond ranges, respectively. Adding such specialized hardware substantially increases the cost of typically resource-constrained sensor nodes. Acoustic systems [6][7] such as Cricket [8] use ultrasonic pulses sufficiently robust to overcome indoor multipath interference but are severely limited by the line-of-sight problem. Further, acoustic signals have limited propagation range.

The recently proposed Radio Interferometric Positioning System (RIPS) [9][10][11] is a promising and inexpensive alternative to UWB systems. The RIPS provides excellent positional accuracy and sensing range in outdoor environments using inexpensive and readily available sensor nodes such as MICA2 motes. However, RIPS is unsuitable for indoor environments because its RF interferometric ranging technique can be severely affected by indoor multipath interference. A modified RIPS system developed by Kusy *et al.* [12][13] used RF Doppler shifts to estimate the direction of moving targets. Kusy reported that frequency change from Doppler shifts was noise-resistant to multipath interference and thus more appropriate for indoor localization. However, their experiments were limited to outdoor environments. Additionally, since the technique detects moving targets by Doppler shifts, their technique falls back to the original RIPS for locating stationary or slow-moving targets.

SenSys'08, November 5–7, 2008, Raleigh, North Carolina, USA.

This study proposes an inexpensive yet highly precise RF-based indoor localization system with sub-meter positional accuracy which is less susceptible to indoor multipath interference than current localization systems. The proposed approach employs spinning beacons anchored in the infrastructure to produce predictable and distinguishable Doppler signals for high-precision localization. Putting spinning motion in the infrastructure brings an additional advantage that the produced Doppler shifts can be used to locate stationary or slow-moving indoor targets. The SpinLoc system was designed and implemented as an actual localization system, and its performance was tested in an indoor garage environment with a ceiling height of approximately 3 meters. The experimental results revealed a median positional error of 40~50 centimeters and a 90% error of 70~90 centimeters.

Two important contributions of this work are the followings:

- Rather than relying on the dynamic movement of mobile targets to produce irregular, variable Doppler shifts as proposed by Kusy *et al.* [6], SpinLoc reverses this setting by instead relying on the spinning motions of selective infrastructure nodes to produce predictable, distinguishable Doppler signals for high-precision localization.
- A novel *Doppler-angulation* method was developed to accurately estimate the angle of a target relative to a spinning beacon. An angle from a spinning beacon with known location fixes a straight line that passes through/nearby the target. By using more than two spinning beacons to produce multiple lines, the target can be localized from the intersection of these lines.

The rest of this paper is organized as follows. Section 2 describes the SpinLoc approach. Section 3 explains the SpinLoc positioning system. Section 4 discusses parametric tuning and performance tradeoff. Section 5 details SpinLoc implementation. Section 6 describes the experimental setup and results. Section 7 reviews the related work. Section 8 describes error sources in SpinLoc. Section 9 discusses the characteristics of SpinLoc. Finally, Section 10 concludes the study and suggests directions for future studies.

2. SPINLOC APPROACH

Two phases of the SpinLoc method are (1) angulation phase and (2) localization phase. The angulation phase measures the Doppler signal from a target and a reference node to a spinning beacon. The difference in observed Doppler shifts reveals the angle between the target and the reference node to the spinning beacon[1]. Such angulation is applied repeatedly to several different spinning beacons. The location of the reference node, the location of the spinning beacon and the estimated angle are then used to determine the probable position of the target. The position of the target can be found by intersecting lines drawn from estimated angles to different spinning beacons in the localization phase. The subsections below describe the Doppler Effect, the proposed technique for deriving angular information and, finally, the localization algorithm based on angular information.

2.1 Doppler Effect

The Doppler Effect refers to the perceived variation in frequency and wavelength given the velocity of a moving object relative to a wave source. Since the speed of a radio wave c is much greater than the relative velocity between the wave source and the observer, the frequency shift Δf, also known as the Doppler shift, can be expressed as

$$\Delta f = \frac{v}{c} f \quad (1)$$

where f denotes the transmitted frequency, and v is the velocity of the wave source relative to the observer. The relative velocity v is negative when the wave source is moving away from the observer. As Figure 1 shows, if the wave source is not moving directly toward/away from the observer, the relative velocity v in Equation (1) should be replaced by the projected velocity on the line connecting the observer and wave source.

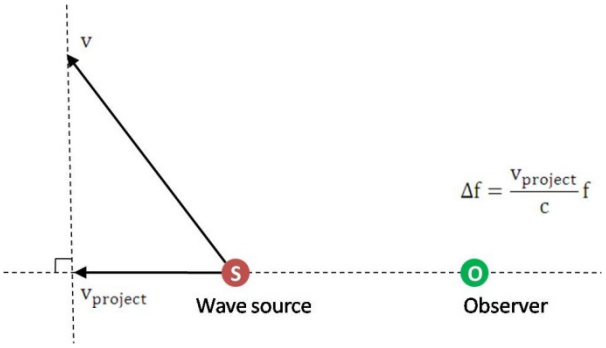

Figure 1. Illustration of Doppler Effect.

2.2 Doppler-Angulation

Doppler-angulation is the proposed method for determining the angle between a stationary target and a reference node to a spinning beacon. This angle is referred to as the orientation angle. Figure 2 illustrates the concept of the Doppler-angulation method where X is the stationary target at distance d from origin O, and the direction from origin O to X is angle α. The position vector of target X is:

$$\overrightarrow{OX} = (d \cdot cos\alpha,\ d \cdot sin\alpha) \quad (2)$$

[1] The location of a spinning beacon refers to the centre of its spinning perimeter.

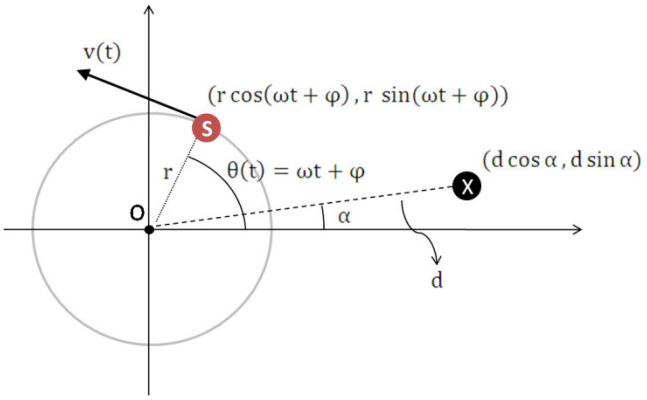

Figure 2. Illustration of Doppler-angulation.

The S is the spinning beacon or a wave source rotating counterclockwise around the origin O at a constant angular velocity ω with a rotational radius r. To maintain generality, the polar angle of S is denoted as $\theta(t)=\omega t+\varphi$. Note that the polar angle of S is the angle included by $\overrightarrow{OS}$ and the positive x-axis. At time t, the position vector of S is:

$$\overrightarrow{OS} = (r \cdot cos(\omega t+\varphi),\ r \cdot sin(\omega t+\varphi)) \tag{3}$$

The tangent line velocity vector $\boldsymbol{v}(t)$ of the beacon S is

$$\boldsymbol{v}(t) = (-\omega r \cdot sin(\omega t+\varphi),\ \omega r \cdot cos(\omega t+\varphi)) \tag{4}$$

According to Equation (1), the observed Doppler shift is proportional to the projected velocity on the line between the spinning beacon and the target. In Figure 2, the vector of the target-beacon connection is $\overrightarrow{SX}$, so the velocity projected on $\overrightarrow{SX}$ is the inner product of $\boldsymbol{v}(t)$ and the unit vector of $\overrightarrow{SX}$:

$$v_{project} = \boldsymbol{v}(t) \cdot \frac{\overrightarrow{SX}}{\left|\overrightarrow{SX}\right|} \tag{5}$$

Equations (2), (3) and (4) are then substituted into Equation (5) to obtain the projected velocity:

$$\begin{aligned} v_{project} &= \boldsymbol{v}(t) \cdot \frac{\overrightarrow{SX}}{\left|\overrightarrow{SX}\right|} = \boldsymbol{v}(t) \cdot \frac{\overrightarrow{OX}-\overrightarrow{OS}}{\left|\overrightarrow{OX}-\overrightarrow{OS}\right|} \\ &= (-\omega r \cdot sin(\omega t+\varphi),\ \omega r \cdot cos(\omega t+\varphi)) \cdot \\ &\quad \frac{(d \cdot cos\alpha,\ d \cdot sin\alpha) - (r \cdot cos(\omega t+\varphi),\ r \cdot sin(\omega t+\varphi))}{\left|(d \cdot cos\alpha,\ d \cdot sin\alpha) - (r \cdot cos(\omega t+\varphi),\ r \cdot sin(\omega t+\varphi))\right|} \\ &= \frac{-\omega r d \cdot sin(\omega t+\varphi)cos\alpha + \omega r d \cdot cos(\omega t+\varphi)\, sin\alpha}{\sqrt{d^2 + r^2 - 2dr \cdot cos(\omega t+\varphi)\, cos\alpha - 2dr \cdot sin(\omega t+\varphi)\, sin\alpha}} \\ &= \frac{-\omega r d \cdot sin(\omega t+\varphi-\alpha)}{\sqrt{d^2 + r^2 - 2dr cos(\omega t+\varphi-\alpha)}} \end{aligned} \tag{6}$$

According to Equation (1), the Doppler shift of the projected velocity is:

$$\begin{aligned} \Delta f &= \frac{v_{project}}{c} f \\ &= \frac{f}{c} \frac{-\omega r d \cdot sin(\omega t+\varphi-\alpha)}{\sqrt{d^2 + r^2 - 2dr\, cos(\omega t+\varphi-\alpha)}} \\ &= \frac{-\omega r d f}{c} \frac{sin(\omega t+\varphi-\alpha)}{d\sqrt{1 + (r/d)^2 - 2(r/d) cos(\omega t+\varphi-\alpha)}} \\ &= \frac{-\omega r f}{c} \frac{sin(\omega t+\varphi-\alpha)}{\sqrt{1 + (r/d)^2 - 2(r/d) cos(\omega t+\varphi-\alpha)}} \end{aligned} \tag{7}$$

If the rotational radius is minor in comparison to the distance from origin O to target X, namely r/d approximates 0, the Doppler shift can be formulated as:

$$\begin{aligned} \lim_{r/d \to 0} \Delta f &= \lim_{r/d \to 0} \frac{-\omega r f}{c} \frac{sin(\omega t+\varphi-\alpha)}{\sqrt{1 + (r/d)^2 - 2(r/d) cos(\omega t+\varphi-\alpha)}} \\ &= \frac{-\omega r f}{c} sin(\omega t+\varphi-\alpha) \end{aligned} \tag{8}$$

The effect of this approximation error on the orientation angle estimation can be mitigated by our system. This mitigating effect is discussed further in Section 4 and Appendix A.

According to Equation (4), when r/d approaches 0, the Doppler shift produces a sine wave with a phase left-shift by an angle $(\varphi-\alpha)$. This sine wave is referred to as the *frequency waveform*. If the Doppler shift can be measured, the angle $(\omega t+\varphi-\alpha)$ can be determined. However, as Figure 3 shows, due to the difficulty of measuring t and φ, an additional reference node with known location is deployed to derive angle $(\omega t+\varphi-\beta)$. In Figure 3, R is the reference node, and X is the target. Polar angles of X and R are denoted as α and β, respectively. Subtracting $(\omega t+\varphi-\alpha)$ from $(\omega t+\varphi-\beta)$ obtains $(\alpha-\beta)$. Identifying the location of R reveals the angle β, which then reveals the direction of X.

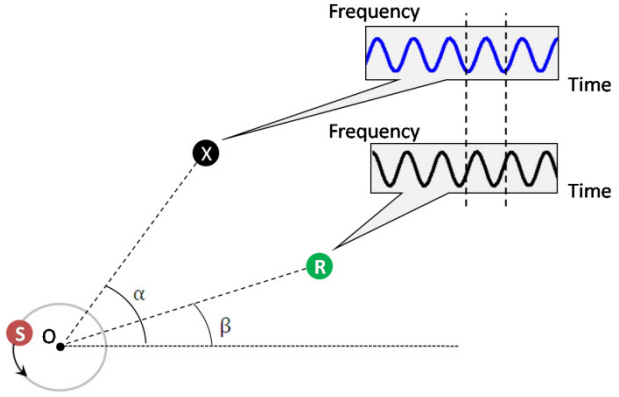

Figure 3. Illustration of Doppler-angulation. The reference node R is deployed to obtain the direction of X.

2.3 Localization Algorithm

Figure 4 shows the localization algorithm where X is the target and S_1 and S_2 are two spinning beacons at known locations. Once the angles θ_1 and θ_2 are measured, the target can be located at the intersection of the two orientation lines. The orientation line extends from the spinning beacon outward in the direction of θ_1 and θ_2. To enhance accuracy in a noisy environment, a robust positioning system would usually require more than two spinning beacons. If the angle measurement is noiseless, all orientation lines would ideally intersect at only one point. However, perfect sensor accuracy is unlikely under real world conditions. Therefore, the actual intersection may resemble that in Figure 4(b). The problem of identifying the most probable location of the target was thoroughly explored in [14][15].

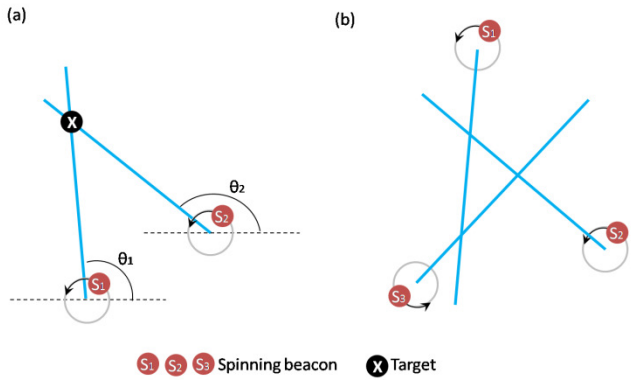

Figure 4. Localization algorithm locates a target at the intersection of multiple orientation lines.

3. SPINLOC POSITIONING SYSTEM

Figure 5 illustrates an example of a deployed SpinLoc positioning system. The example deployment in Figure 5(a) contains the following sensor nodes: (1) target X, (2) reference node R and (3) three spinning beacons S_1, S_2 and S_3. Since S_1, S_2, S_3 and R are stationary infrastructure nodes at known locations, the SpinLoc positioning system must locate target X. The SpinLoc localization process involves the following four steps:

(1) Doppler shifted signal generation: While spinning, S_1 transmits RF signals at a constant frequency. X and R then measure Doppler shifted signals resulting from the spinning motion of the transmitter S_1.

(2) Frequency record: Both X and R record the Doppler shifted signals received from S_1 and then send their observed frequency waveforms to the base station.

(3) Orientation angle calculation: As described above, the base station applies the Doppler-angulation method which takes the observed frequency waveforms of X and R and calculates their orientation angle to S_1. As Figure 5(b) shows, since the locations of both S_1 and R are identified, the orientation line passing through/nearby X can be obtained.

(4) Location estimation: Figure 5(c) shows that after repeating steps *(1)* ~ *(3)* for S_2 and S_3, two additional blue orientation lines passing through/near the position of X are obtained. The location of X is then estimated by finding the intersection of these three lines.

Each of these four steps is described in detail in the following subsections.

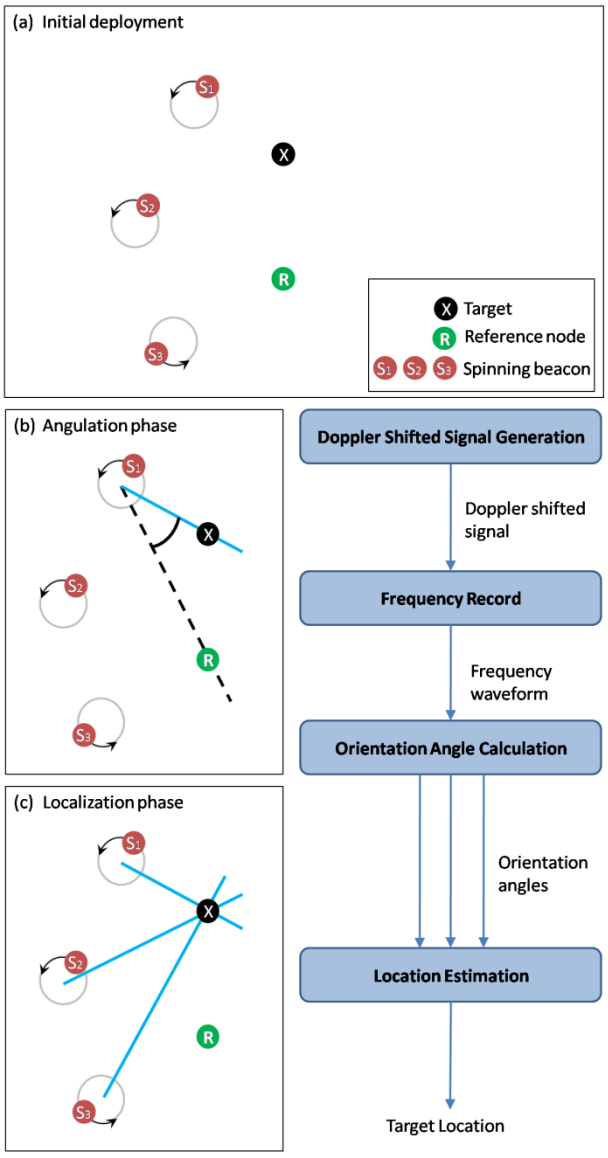

Figure 5. Deployment of the SpinLoc positioning system: (a) deployment layout, (b) angulation phase and (c) localization phase.

3.1 Doppler Shifted Signal Generation

The first step is to generate Doppler shifted signals. A beacon embedded with a RF transceiver module transmits radio signals while spinning. However, a typical RF carrier frequency in the 400 MHz ~ 2.4 GHz range is too high for analysis by a hardware-constrained sensor node due to its slow clock and limited sampling rate. The radio interferometry method developed by Maroti *et al.* [9] is therefore used to overcome such limitations. Radio interferometry measures RF Doppler shift with sufficient accuracy using inexpensive sensor hardware such as MICA2 motes and is used in the system as follows. First, two sensor nodes simultaneously transmit sine waves at two very similar high radio frequencies f_1 and f_2. The similarity of the two RF signals produces an interference RF signal with a low frequency envelope $|f_1-f_2|$. For example, two high frequency 900 MHz radios can transmit sine waves at slightly different frequencies to produce a low interference frequency envelope below 1 kHz, which is slow enough for analysis by a MICA2 mote.

Radio interferometry requires simultaneous transmissions from two radios. Therefore, as Figure 6 shows, a static assistive beacon is required. The spinning beacon transmits RF signals at its original frequency (f_1) and any receiver P will perceive radio frequency at f_1 plus a Doppler shift (Δf_1^P). The assistive beacon simultaneously emits signals at a fixed frequency (f_2). Since the assistive beacon is stationary, the interference frequency, *i.e.*, $|f_1-f_2+\Delta f_1^P|$, is affected only by the Doppler shift in the signal frequency of the spinning beacon. Fine-tuning the Doppler shifted interference frequency $|f_1-f_2+\Delta f_1^P|$ to a low frequency range under 1 kHz enables detection and analysis of the signal by a MICA2 mote.

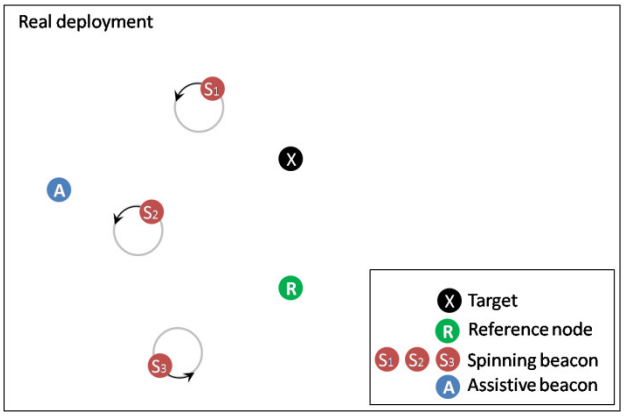

Figure 6. An example deployment of SpinLoc system. An assistive beacon is added after initial deployment.

3.2 Frequency Record

The second step is for X and R to record their received Doppler shifted frequencies from S_1. X and R receive radio frequencies and analyze them by RSS analog-to-digital converter (ADC) on sensor nodes. The real-time time-domain frequency estimation method proposed by Maroti *et al.* [9] is used to detect the RSS peak timestamps and estimate the interference frequency. For example, if the RSS sampling rate is 17,800 Hz and the number of samples between adjacent RSS peaks is 30, the interference frequency is approximately 17,800/30 = 593.3 Hz. Receiver nodes X and R send their RSS peak timestamps to the base station where the timestamps are then analyzed to reconstruct their frequency waveforms.

3.3 Orientation Angle Calculation

The third step is to calculate the orientation angle using the frequency waveforms of X and R. Specifically, as Figure 5(b) shows, this orientation angle is the angle between nodes R and X relative to spinning beacon S. A simple method of calculating this orientation angle is to use the Doppler-angulation method described in subsection 2.2. First, by using radio interferometry, we measure the frequency shift value perceived by X and R. Second, this frequency shift value is used to determine angle $(\alpha-\beta)$ in Figure 3. If X and R reveal Doppler shifts Δf_x and Δf_R, respectively, at time t, $(\alpha-\beta)$ can be calculated as follows. First, Δf_x is substituted into Equation (8):

$$\Delta f_x = \frac{-\omega r f}{c} \sin(\omega t+\varphi-\alpha)$$
$$\frac{-c\Delta f_x}{\omega r f} = \sin(\omega t+\varphi-\alpha) \quad (9)$$

By taking the arcsine function on both sides of the Equation (9), α is determined:

$$\sin^{-1}\left(\frac{-c\Delta f_x}{\omega r f}\right) = \omega t+\varphi-\alpha$$
$$\alpha = \omega t+\varphi-\sin^{-1}\left(\frac{-c\Delta f_x}{\omega r f}\right) \quad (10)$$

Similarly, β is computed as follows:

$$\beta = \omega t+\varphi-\sin^{-1}\left(\frac{-c\Delta f_R}{\omega r f}\right) \quad (11)$$

The angle $(\alpha-\beta)$ is obtained by simply subtracting Equation (11) from Equation (10):

$$\alpha-\beta = \sin^{-1}\left(\frac{c\Delta f_R}{\omega r f}\right)-\sin^{-1}\left(\frac{c\Delta f_x}{\omega r f}\right) \quad (12)$$

Although the above solution is simple and mathematically sound, one practical problem arises in an actual working system and environment. The radio on a MICA2 mote can only be tuned at a resolution of 65 Hz. Restated, the actual transmitted and received frequencies would have errors of plus/minus 65 Hz. These errors reduce precision when determining the value of actual transmitted frequency f on the spinning beacon S. On the receiver nodes X and R, these errors also cause imprecise measures of Doppler shifts Δf_x

and Δf_R. In other words, although using a finer resolution and more expensive radio chip on a beacon (infrastructure) could improve the accuracy of actual transmitted frequency f from S, the measured Doppler shifts, *i.e.*, Δf_x on X and Δf_R on R, would remain imprecise.

Instead, a more precise measure is the overall shifted interference frequency, which is the sum of the base interference frequency and Doppler shift. Although Equation (12) cannot directly solve $(\alpha-\beta)$ with the Doppler shift at some instant t, analysis of Doppler frequency shifts over a given time period can solve $(\alpha-\beta)$ more robustly.

According to Equation (8), Δf_x and Δf_R can be regarded as functions of time t as follows:

$$\begin{cases} \Delta f_x(t) = \dfrac{-\omega r f}{c} \sin(\omega t+\varphi-\alpha) \\ \Delta f_R(t) = \dfrac{-\omega r f}{c} \sin(\omega t+\varphi-\beta) \end{cases} \quad (13)$$

As Equation (13) shows, $\Delta f_x(t)$ and $\Delta f_R(t)$ are both sinusoidal waves with the same periodicity but with a relative phase offset $(\alpha-\beta)$. Figure 7 shows the actual measured interference frequency shifts $\Delta f_x(t)$ and $\Delta f_R(t)$ where y-axis is the Doppler shifted interference frequency. Further observation reveals that the problem of solving for $(\alpha-\beta)$ is equivalent to identifying the phase shift between the measured $\Delta f_x(t)$ and $\Delta f_R(t)$.

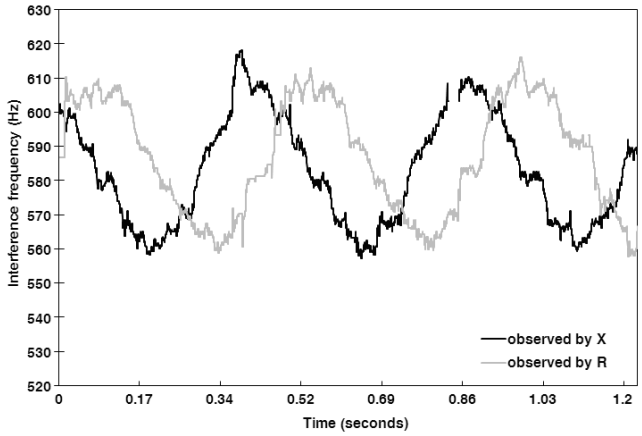

Figure 7. Example of observed Doppler shifted frequencies.

A common problem in digital signal processing is identifying phase shift in two discrete-time noisy sinusoid signals with the same periodicity [16]. Let $X[n]$ and $Y[n]$ denote two discrete-time noisy sinusoid signals with the same period N. A common solution is to delay $Y[n]$ by time k and compare the similarity between $X[n]$ and $Y[n-k]$, where $Y[n-k]$ is the same as $Y[n]$ with a right shift of time k. The phase offset can be calculated from time k such that $X[n]$ is most similar to $Y[n-k]$ as follows:

$$2\pi \frac{k}{N} \quad (mod\ 2\pi) \quad (14)$$

The sum squared differences (SSD) [16] is selected as the distance function required to quantitatively express the similarity of two signals. The SSD of $X[n]$ and $Y[n-k]$ is defined as:

$$\sum_{n=-\infty}^{\infty} \left(X[n]-Y[n-k]\right)^2 \quad (15)$$

In any implementation, one can only observe the shifted frequencies for a limited time period T. Therefore, SSD is normalized by the overlap in duration of each delay unit k:

$$D_{XY}[k] = \sqrt{\frac{\sum_{n=k}^{T-1} \left(X[n]-Y[n-k]\right)^2}{T-k}} \quad (16)$$

The square root is calculated so that $D_{XY}[k]$ accurately defines distance. The resulting k value is such that $D_{XY}[k]$ is the minimum for $k=0$ to $T-1$. Excessive noise in $\Delta f_x(t)$ and $\Delta f_R(t)$ may yield unreasonably high $D_{XY}[k]$ values. Therefore, to avoid false estimations under these conditions, a threshold is applied to filter estimations from excessively noisy signals. The effect of the filter at different thresholds is evaluated in Section 6. The calculated phase offset yields the orientation line for location estimation.

3.4 Location Estimation

Since three spinning beacons are used in the example deployment, Doppler-angulation calculates three orientation angles and three corresponding lines toward the target. However, as Figure 4(b) shows, varying angular errors affect varying shifts in these orientation lines away from the target. These shifts bring the three orientation lines to intersect at three different points rather than at the same point.

Given multiple intersection points, a target can be located by several different algorithms. For example, the Centroid algorithm locates the target at the Centroid of these three intersection points. SpinLoc proposed here uses the Weighted Centroid algorithm, which weights each intersection point according to an internally computed confidence value. This confidence value is proportional to the acuteness of the intersection angle between two intersecting orientation lines because the acuteness angle affects the sensitivity of angular error on positional error. For example, as Figure 8 shows, when the intersection angle is close to 0 or 180 degrees, even a minor angular error can produce a large positional error. Note that the x-axis and y-axis error sensitivities for each intersection point differ and are considered separately.

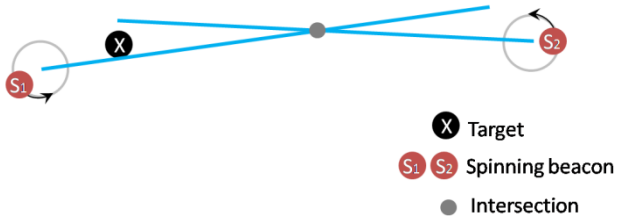

Figure 8. Example of a minor angular error causing a large positional error.

4. PARAMETRIC TUNING AND PERFORMANCE TRADEOFF

Different value settings of tunable parameters determine overall system performance. The main system performance metrics considered are *positional accuracy* and *positioning latency*. Positional accuracy measures the difference between an estimated location and a ground-truth location. Positioning latency is the time required for SpinLoc to measure and estimate a position. The tunable system parameters are (1) Doppler-angulation filtering threshold, (2) data collection time, (3) rotational velocity, (4) interference frequency and (5) rotational radius. Generally, tuning these parameters improves accuracy but at the expense of prolonged latency, and vice versa. Restated, adjusting these parameters determines the performance tradeoff between accuracy and latency.

(1) Doppler-angulation filtering threshold: The delay-and-compare process described in subsection 3.3 has the following two outputs: estimated time delay k and minimum distance $D_{XY}[k]$ between two input signals. The minimum distance reveals the quality of the estimation. A smaller minimum distance indicates a more reliable time delay estimation. Therefore, before using the measured angular information to localize the target, poor angular estimation is filtered out as noise according to the minimum distance. Since the stricter filtering threshold removes more noise from the dataset, it produces a more accurate angulation result. Although a stricter filtering threshold increases overall positioning latency, it also prolongs the positioning latency to acquire enough high-quality orientation angle estimates.

(2) Data collection time: A longer data collection time increases the number of signal samples, which enables more precise reconstruction of frequency waveforms and improves positional accuracy. However, the tradeoff is increased positioning latency. Notably, an overly long data collection time has adverse effects such as increased carrier frequency drift and clock drift.

(3) Rotational velocity: An instantaneous radio frequency is difficult to detect when rotational velocity is high because of the shorter time that a rapidly spinning beacon is positioned in a specific direction. Faster rotation reduces the number of signal samples collected and thus reduce the precision of frequency waveform detection, which increases positional error. However, high rotational velocity improves positioning latency because it provides more signal samples for Doppler-angulation. Note that a very slow rotational velocity may also produce a large positional error because frequency waveforms of small Doppler shifts are more difficult to distinguish.

(4) Interference frequency: Because of the Doppler Effect and the characteristics of radio interferometry, a higher interference frequency increases the Doppler shift, which also improves the signal-to-noise ratio (SNR) of the frequency waveform. However, a high interference frequency also has certain disadvantages. For example, if the interference frequency is 500 Hz and the signal sampling rate is 17,800 Hz, the number of signals sampled per period is 17,800/500 = 35.6. When the interference frequency increases to 1,000 Hz, the number of signals sampled per period is halved to 17,800/1,000 = 17.8. Fewer signal samples degrade the precision of the frequency detection in radio interferometry, thus affecting the positional accuracy of the SpinLoc system.

(5) Rotational radius: A long rotational radius (r) and a high angular velocity (ω) of a spinning beacon produce large Doppler shifts because, as Figure 2 shows, the tangent line velocity ($v(t)$) is the product of r and ω. Further, large Doppler shifts produce more distinguishable frequency waveforms, which improve the SNR of the frequency waveform and reduce positional error. However, a long rotational radius also has disadvantages. A long rotational radius (r) not only requires a larger physical space, it also, as Equation (8) shows, increases the approximation error in Equation (8) as the r/d ratio increases. Fortunately, the effect of the approximation error is mitigated by the proposed method of estimating the orientation angle. The proposed method of identifying phase shift in two Doppler shifted frequency signals is not sensitive to r/d ratios. Varying the r/d pairs numerically simulates two non-approximated waveforms from Equation (7) when performing the orientation angle calculation, where r/d ratio pair (0, 0) stands for the approximated case. The analytical results show that, whether or not they are approximated, the calculated orientation angles are identical. Appendix A provides a detailed example of the calculation.

These parametric tradeoffs are experimentally analyzed in Section 6.

5. IMPLEMENTATION

The proposed SpinLoc system was implemented on MICA2 motes manufactured by Crossbow Inc. These MICA2 motes ran TinyOS. One MICA2 mote was connected to a base station via MIB520 programming board to relay packets containing frequency waveforms from infrastructure nodes and the target. These MICA2 motes were programmed to emit pure sine waves, which produced Doppler shifts when transmitted from the rotating beacons. The

RIPS engine developed by Vanderbilt University [17] was modified and ported to 900 MHz MICA2 motes. At our test site location in Taiwan, the frequency band of GSM-900 [18] also happens to be around 900MHz, overlapping with a part of MICA2 radio channels. To avoid interference from the GSM-900 up/down link channels, we selected 18 carrier frequencies between 821.277MHz to 921.337MHz whose ranges are away from GSM-900 channels.

Additionally, as Figure 9 shows, each spinning beacon was mounted on the arm of a rotation device. The rotation device, consisting of a motor for spinning an attached arm and a control unit with adjustable rotational velocity, was securely mounted on a steel platform. The cost of each rotation motor/device is about 100 US dollars. Industry-grade servo motors, such as [19] with almost one million hours MTBF (Mean Time Between Failures), can also be used to build robust rotation devices. Changing rotational velocity produced varying Doppler shifts.

In each measurement round, the base station transmits a command to all sensor nodes. After performing time synchronization, the spinning and assistive beacons transmit radio signals while the reference node and the target log and send received signal frequencies to the base station. After receiving the signal frequencies, the base station calculates the orientation angle for each spinning beacon and estimates the position of the target.

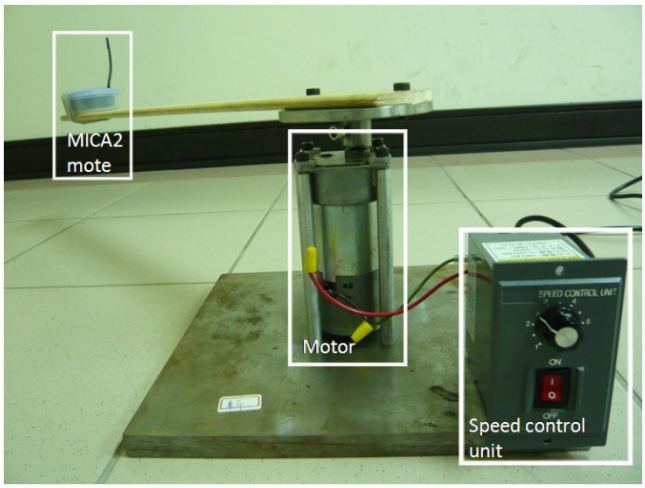

Figure 9. Rotation device consisting of motor, speed control unit and steel platform for stability.

6. EXPERIMENTAL RESULTS

As Figure 10 shows, the system was tested in an indoor parking garage in the basement of a university building. The parking garage had a ceiling height of 3 meters, and MICA2 motes were deployed over an 8×10 m^2 area.

The infrastructure components included three spinning beacons, one reference node and one assistive beacon. Figure 11 shows the positions of these infrastructure nodes. The grid points on the map are 2 meters apart. To measure positional accuracy throughout this test environment, a target was moved among the thirty different grid points on the map.

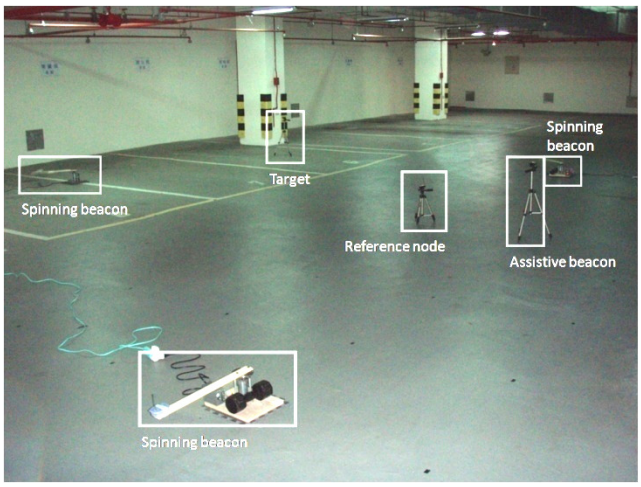

Figure 10. Indoor parking garage environment with infrastructure node deployment.

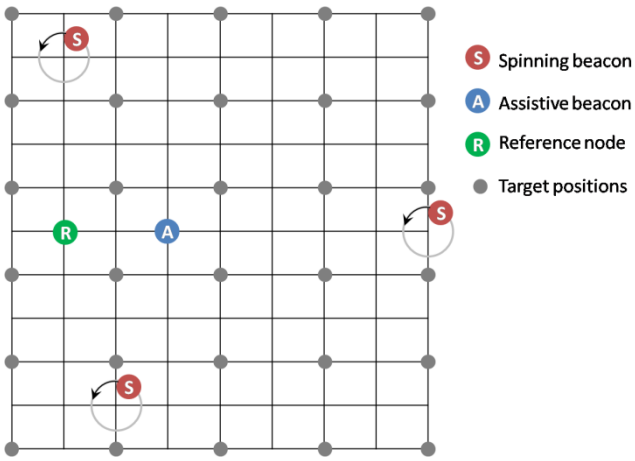

Figure 11. Grid map of infrastructure node positions.

6.1 SpinLoc Positional Errors

Figure 12 shows the cumulative density function (CDF) of the positional errors. The parametric settings were as follows: rotational radius was 50 centimeters, angular velocity was 133 revolutions per minute (RPM), interference frequency was 600 Hz, and data collection time was 1.5 seconds. The median positional error was 39 centimeters, and the 90% error is 70 centimeters (meaning 90% of errors were 70 centimeters or less). The test results demonstrated that the SpinLoc system achieves sub-meter positional accuracy in an indoor environment.

Figure 13 depicts the cumulative density function (CDF) of absolute angular error with a median error of 3 degrees and 90% of errors 10 degrees or less. The dataset for the CDF was based on 300 sample position estimates over the thirty grid points (ten samples per grid point). Since each positioning sample is derived from three estimated angles, 900 angle estimates were sampled. Although some angular errors were seemingly large, their effects on positional accuracy were mitigated in the localization phase because these large errors could be identified as outliers by analyzing the intersection of multiple orientation lines measured by multiple spinning beacons.

Figure 14 shows the probability distribution function (PDF) of angular errors from the same dataset in Figure 12 without taking absolute values. The figure shows that angular errors were equally distributed between positive and negative.

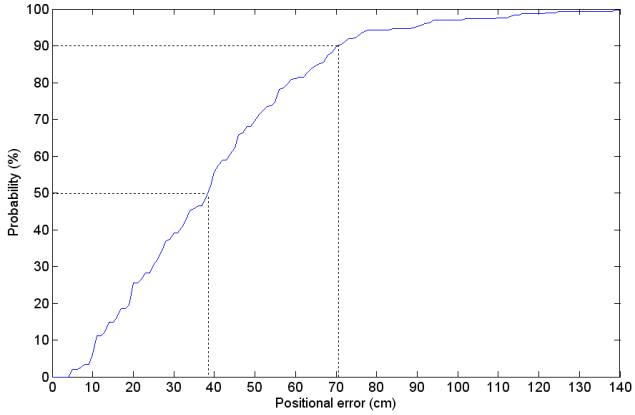

Figure 12. CDF of positional errors.

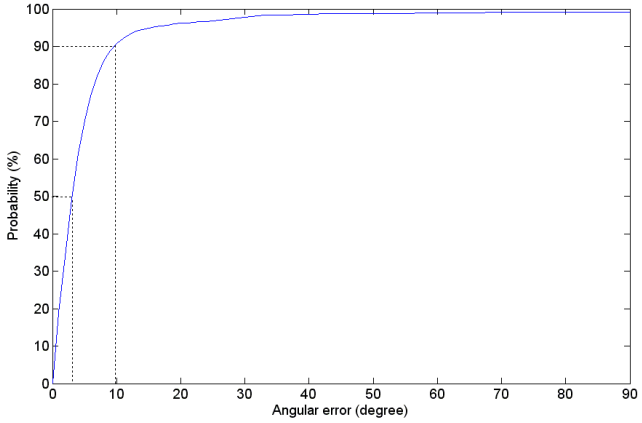

Figure 13. CDF of angular errors.

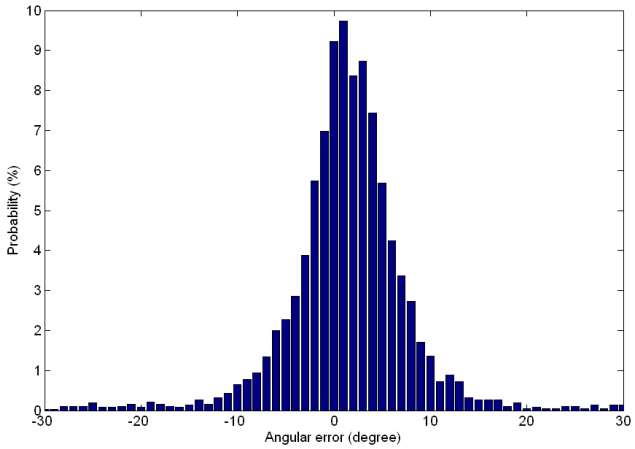

Figure 14. PDF of angular errors.

6.2 Doppler-Angulation Filtering

Figure 15 shows the relationship between angular errors and filtering thresholds from 5 (stricter) to 15 (less strict) as well as the relationship between data reduction % and filtering thresholds. Clearly, without the noise filtering, angular errors were relatively large (see "No filter" in the *x*-axis of Figure 15). However, at the strictest noise filtering threshold, the system removed almost 80% of the received packets. Our system was deployed with a filtering threshold value set at 10, which was sufficient to reduce most of noisy data. Figure 16 shows the corresponding CDF of angular errors under different filtering thresholds.

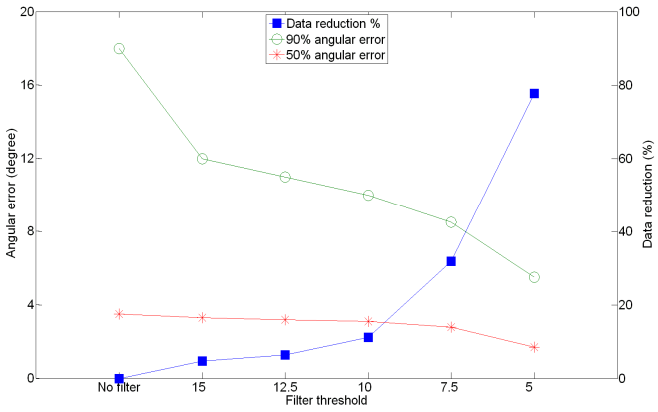

Figure 15. Angular errors and filtered out data ratios under different filtering thresholds from none to 5.

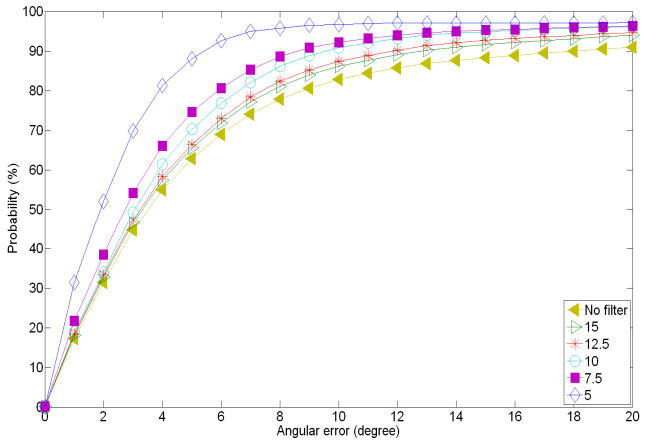

Figure 16. CDF of the angular errors under different filtering thresholds. The lines from right to left are in the order from 'No filter' (top) to 5 (bottom) in the legends.

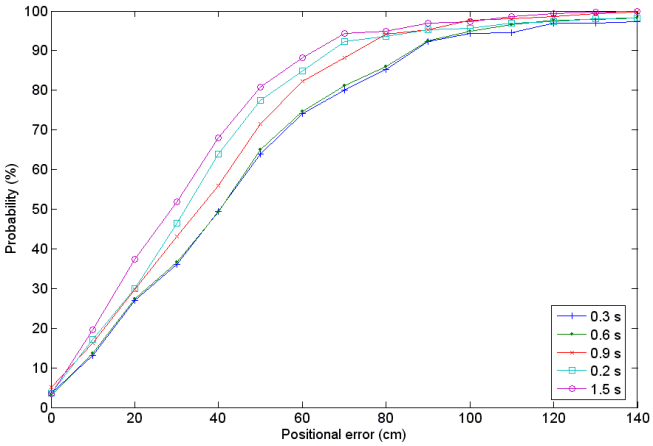

Figure 18. CDF of the positional errors under different data collection times. The lines from right to left are in the order from 0.3s (top) to 1.5s (bottom) in the legends.

6.3 Data Collection Times

Figure 17 shows the positional errors at different length of data collection times (0.3 ~ 1.5 seconds). Two curves plot the median positional errors and 90% positional errors. The analytical results show that a longer data collection time generally reduces positional error because the increased number of signal samples enables more accurate reconstruction of frequency waveforms. At the shortest data collection time of 0.3 second, the SpinLoc system still achieved sub-meter accuracy with 90% positional error of 93 centimeters. Figure 18 depicts the corresponding CDF of positional errors for different data collection times ranging from 0.3 to 1.5 seconds.

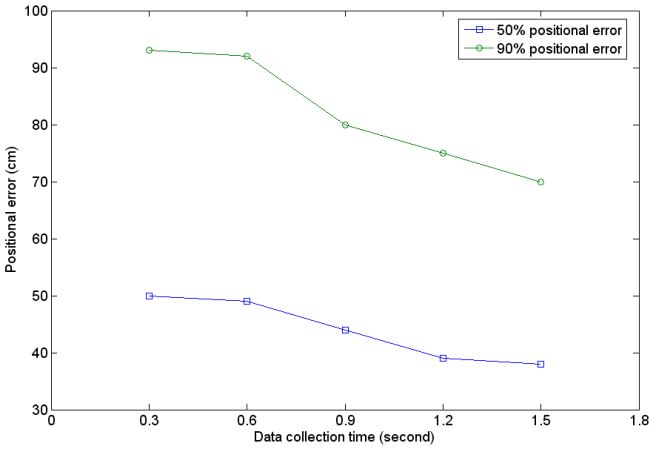

Figure 17. The median and 90% positional errors under different data collection times from 0.3 to 1.5 seconds.

6.4 Rotational Velocities

Figure 19 shows the angular errors of different rotational velocities of the spinning beacon varying from 92 to 200 RPM. The 120-150 RPM range achieved the best accuracy with a median error of about 3 degrees and a standard deviation of approximately 1 degree. As described in Section 4, excessively fast velocities are undesirable due to the insufficient number of signal samples for reconstructing frequency waveforms, and excessively slow rotational velocities are also undesirable due to the less distinguishable frequency waveforms from the smaller Doppler shifts.

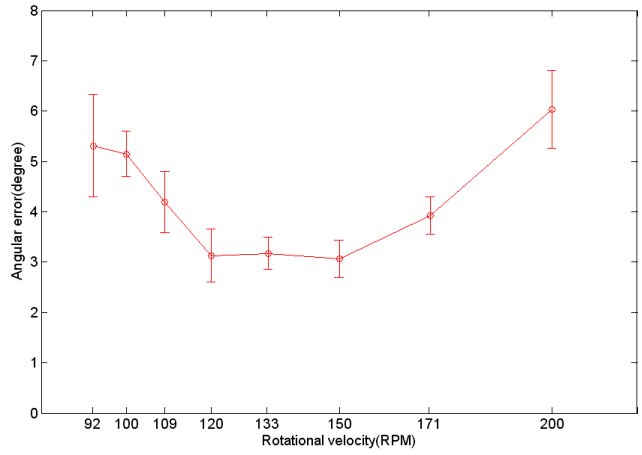

Figure 19. Angular errors under rotational velocities varying from 92 to 200 RPM.

6.5 Interference Frequency

Figure 20 shows the angular errors under different interference frequencies (100 ~ 1,200 Hz). The interference test results suggested that the optimal interference frequency range is between 200 Hz and 1,000 Hz. The proposed system used the interference frequency of 600 Hz, which is in the middle of this range.

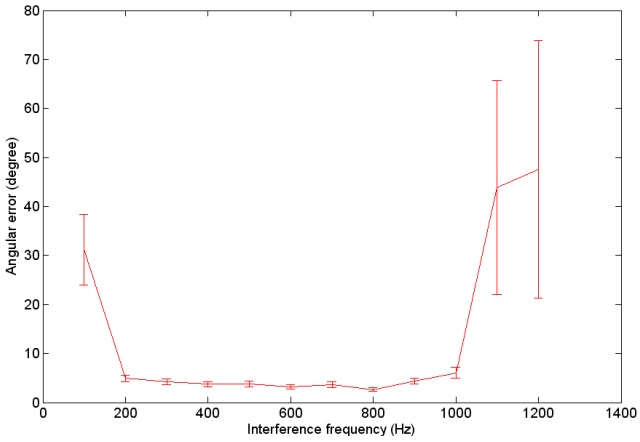

Figure 20. Angular errors under different interference frequencies from 100 Hz to 1,200 Hz.

7. ERROR SOURCES

The errors were due to varying factors such as MICA2 mote hardware limitations, the inevitable indoor multipath interference and errors inherited from the radio interferometry technique. These error sources are discussed further below.

(1) Time synchronization error: Time synchronization errors can be controlled by clock rate. Although SpinLoc eliminates the need to synchronize the spinning beacon with receiver nodes, the receiver nodes must still be synchronized with each other so that frequency waveforms from different receiver nodes can be compared and analyzed to determine their phase shift. When the data collection time is much longer than the synchronization error, this source of error can be minimized. Clock drift may contribute to positional error because synchronization is performed only at the beginning of each data collection cycle.

(2) Carrier frequency drift: This error may be caused by the MICA2 motes hardware, as described in [9]. Although reducing the data collection time can minimize frequency drift, the number of signal samples collected may be insufficient for precise reconstruction of frequency change waves. However, since the system analyzes Doppler waveforms rather than actual frequencies, carrier frequency drift has only minor effects on system performance.

(3) Indoor multipath interference: An advantage of working in the frequency domain is that reflection wave remains the same frequency as the incident wave. However, this advantage applies only to a static wave source. When the wave source is moving, Doppler Effect causes the line-of-sight signal and the multipath signals to be at slightly different frequencies. Therefore, the estimated frequency is still affected by the indoor multipath interference.

8. RELATED WORK

The most relevant work is the frequency-difference-of-arrival (FDOA) technique. The FDOA is analogous to time-difference-of-arrival (TDOA) for estimating the location of a radio emitters based on observations from several known points. Such a technique was employed by Kusy *et al.* [13] to track mobile targets by using infrastructure nodes as receivers and targets as beacon emitters. When the target is moving in such a system, each infrastructure receiver observes varying Doppler shifts depending on their positions relative to the moving target. The target location and velocity are then solved by constrained non-linear squares (CNLS) optimization given the input parameters of geometric relationships between nodes, different Doppler shift measurements and the target velocity vector. However, due to signal noise, Kusy reported accurate results in velocity estimation but no positioning estimation. They therefore combined the accurate estimated velocity vector with the Extended Kalman Filter (EKF) in a tracking task, which achieved an average localization error of 1.5 to 3 meters in an outdoor environment. As work developed independently, Ledeczi *et al.* [20] proposed a localization method based on Doppler shifted RF signals from a rotating antenna. Their simulation showed potential for achieving high positional accuracy below 10 centimeters.

The underlying technique used by Kusy *et al.* [13] to measure Doppler shifts with low-cost hardware is the radio interferometry approach used in RIPS [9]. The RIPS approach uses two nodes transmitting RF signals at slightly different frequencies to produce an interference frequency envelop at a low frequency, which can then be measured and analyzed by a low sampling rate ADC on a MICA2 mote. The RIPS measures the relative phase offset of the received interference signals to obtain q-range information, which is the linear combination of distances between the two radio transmitters and the two receivers. Wu *et al.* [21] developed the adaptive RIPS that enhanced the positional accuracy of RIPS by dynamically selecting anchor nodes as beacon senders.

Many other proposed sensor network positioning systems can be broadly classified as ranging-based and ranging-free methods.

(1) Ranging-based methods. These methods commonly require signal communications between an anchor observer and a locating target. The major differences among them are the varying calibration methods and the use of different signal sources, such as sonic, ultrasonic, infrared, camera, RF, etc. For example, Acoustic ENSBox [7] employs a distribution acoustic sensing platform which enables rapid deployment and self-calibration of an acoustic embedded

networked sensing box. The system can reportedly achieve positional accuracy to within 5 centimeters in a partially obstructed 80 × 50 m^2 outdoor environment. Given that signals propagate at constant velocity, time–of-arrival (TOA) methods [22][23] estimate distance by measuring signal propagation time. Angle-of-arrival (AOA) [24] is a network-based solution that exploits the geometric properties of the arriving signal. By measuring the angle at which the signal arrives at multiple receivers, the system can accurately estimate location. The TDOA [25] is another network-based system which infers distance by measuring time differences. Some hybrid approaches of TOA, AOA, and TDOA have also been proposed [26].

Another class of techniques measures the RSS. These techniques exploit the decaying model of electromagnetic fields to translate RSS into a corresponding distance [23][27][28]. The frequency bands used for transmission may also vary. For example, the well-known RADAR system [29] uses RF, and LADAR and SONAR use visible light and audible sound bands, respectively. Other systems such as LADAR and SONAR analyze signals reflected from an object to estimate its location. A recent innovation, Cricket [8], employs a hybrid approach using both RF and ultrasonic bands. However, the propagation characteristics are irregular in actual outdoor environments [30]. Localization systems using RSS information have similar limitations and usually achieve only meter-level accuracy.

(*2) Range-free methods*. These methods use other alternatives to range estimation between anchor nodes to localize targets. For example, APIT [31] estimates the location of targets based on the connectivity information to anchor node with known location. The greater the number of deployed anchor nodes, the greater the accuracy of the technique. Restated, accuracy highly depends on the density of deployed anchor nodes. One class of techniques detects sequences of artificially generated events from an event scheduler. For example, Spotlight [32] and Lighthouse [33] correlate the event detection time of a sensor node with known spatiotemporal relationships. The detection events are then mapped to estimate position. However, generating and disseminating these events in a large-scale area is relatively difficult, particularly given the calibration requirements.

9. DISCUSSION

The following aspects of SpinLoc are discussed: (1) target node scalability, (2) beacon node scalability, and (3) 3D positioning. On the target node scalability, the base station processing time per target localization is 0.47 second. The current algorithm for computing the target localization can be further optimized and parallelized to reduce processing time, hence improves scalability in the number of target nodes.

On the beacon node scalability, since nearby beacons can interfere with each other's transmission, SpinLoc runs a time synchronization protocol on nearby beacons and schedules their transmissions in different time slots to avoid signal interference. This means that increasing the beacon density improves positional accuracy at the cost of prolonged positional latency. More complex scheduling algorithms can be used to improve beacon node scalability.

Although the current SpinLoc system locates targets only in 2D, it is possible to extend SpinLoc to 3D by adding additional beacons that rotate on the vertical plane. Analyzing produced Doppler shifted signals on the vertical plane yields the height of a target.

10. CONCLUSIONS AND FUTURE WORK

The proposed SpinLoc system presents a novel indoor localization method that overcomes indoor multipath interference and achieves sub-meter positional accuracy. The experimental results in an indoor garage environment achieved a median positional error of 39 centimeters and a 90% positional error of 70 centimeters. By using spinning beacons to produce predictable and distinguishable Doppler Effects, the SpinLoc system achieves sub-meter localization accuracy. Additionally, SpinLoc is highly cost effective since its deployment requires only inexpensive hardware available on MICA2 motes.

Our future work will explore more characteristics and further refinements of the SpinLoc system. (1) We are interested in conducting a systematic evaluation to explore the potential relationship between the target's location (e.g., its proximity to a wall, its relative distances to nearby beacons, etc.) and its positional error. (2) Although the current system is effective for tracking stationary or slow-moving targets, it may not work well for tracking fast-moving targets. Hence, we are interested in developing a method that can compensate for the increased Doppler shifts from fast-moving targets. (3) A typical office deployment is likely to have obstructions, such as furniture. We are interested in evaluating the effect of different types of obstructions on the SpinLoc positional accuracy. (4) It is important to design and mask the exterior of these spinning beacons such that their appearance becomes less obtrusive in an office setting. For example, it may be possible to mask a spinning beacon on a ceiling fan.

REFERENCES

[1] A. Harter, A. Hopper, P. Steggles, A. Ward, and P. Webster, "The anatomy of a context-aware application," *in Proc. of 5th ACM International Conference on Mobile Computing and Networking (Mobicom)*, August 1999.

[2] J. Hightower and G. Borriello, "Location systems for ubiquitous computing," *IEEE Computer*, vol.34, no.8, pp.57-66, August 2001.

[3] Ubisense. http://www.ubisense.net

[4] M. Tuchler, V. Schwarz, and A. Huber, "Location accuracy of an UWB localization system in a multi-path

environment," *in Proc. of IEEE International Conference on Ultra-Wideband (ICUWB)*, September 2005.

[5] S. Gezici, Z. Tian, G. B. Giannakis, H. Kobayashi, A. F. Molisch, H. V. Poor, and Z. Sahinoglu, "Localization via ultra-wideband radios: a look at positioning aspects for future sensor networks," *IEEE Signal Processing Magazine*, July 2005.

[6] J. Scott and B. Dragovic, "Audio location: accurate low-cost location sensing," *in Proc. of 3rd International Conference on Pervasive Computing*, May 2005.

[7] L. Girod, M. Lukac, V. Trifa, and D. Estrin, "The design and implementation of a self calibrating acoustic sensing platform," *in Proc. of 3rd ACM International Conference on Embedded Networked Sensor Systems (SenSys)*, October 2006.

[8] N. B. Priyantha, A. Chakraborty, and H. Balakrishnan. "The Cricket location-support system," *in Proc. of 6th ACM International Conference on Mobile Computing and Networking (MobiCom)*, August 2000.

[9] M. Maroti, B. Kusy, G. Balogh, P. Volgyesi, A. Nadas, K. Molnar, S. Dora, and A. Ledeczi, "Radio interferometric geolocation," *in Proc. of 3rd ACM International Conference on Embedded Networked Sensor Systems (SenSys)*, November 2005.

[10] B. Kusy, M. Maroti, G. Balogh, P. Volgyesi, J. Sallai, A. Nadas, A. Ledeczi, and L. Meertens, "Node density independent localization," *in Proc. of 5th International Symposium on Information Processing in Sensor Networks (IPSN/SPOTS)*, April 2006.

[11] B. Kusy, G. Balogh, A. Ledeczi, J. Sallai, and M. Maroti, "inTrack: High precision tracking of mobile sensor nodes," *in Proc. of 4th European Workshop on Wireless Sensor Networks (EWSN)*, January 2007.

[12] B. Kusy, J. Sallai, G. Balogh, A. Ledeczi, V. Protopopescu, J. Tolliver, F. DeNap, and M. Parang, "Radio interferometric tracking of mobile wireless nodes," *in Proc. of 5th International Conference on Mobile systems, applications and services (MobiSys)*, June 2007.

[13] B. Kusy, A. Ledeczi, and X. Koutsoukos, "Tracking mobile nodes using RF Doppler shifts," *in Proc. of 5th ACM International Conference on Embedded Networked Sensor Systems (SenSys)*, November 2007.

[14] C. D. McGillem and T. S. Rappaport, "A beacon navigation method for autonomous vehicles," *IEEE Transactions on Vehicular Technology*, vol.38, no.3, pp.132-139, August 1989.

[15] A. Nasipuri and R. el Najjar, "Experimental evaluation of an angle based indoor localization system," *in Proc. of 5th International Symposium on Modeling and Optimization in Mobile, Ad Hoc and Wireless Networks (WiOpt)*, April 2006.

[16] F. Viola and W.F. Walker, "A comparison of the performance of time-delay estimators in medical ultrasound," *IEEE Transactions on Ultrasonics, Ferroelectrics and Frequency Control*, vol.50, no.4, pp. 392-401, April 2003.

[17] http://tinyos.cvs.sourceforge.net/tinyos/tinyos-1.x/contrib/vu/apps/RipsOneHop/

[18] 3rd Generation Partnership Project, *3GPP TS 05.05*, http://www.3gpp.org/

[19] Tamagawa Seiki Co., Ltd. http://www.tamagawa-seiki.com/english/products/motor/resolver.html

[20] A. Ledeczi, P. Volgyesi, J. Sallai, and R. Thibodeaux, "A novel RF ranging method," in *Proc. of Sixth Workshop on Intelligent Solutions in Embedded Systems (WISES08)*, July 2008.

[21] H. Wu, H. Chang, C. You, H. Chu, and P. Huang, "Modeling and optimizing positional accuracy based on hyperbolic geometry for the adaptive radio interferometric positioning system," in *Proc. of 3rd International Workshop on Location- and Context-Awareness (LoCA),* September 2007.

[22] F. Izquierdo, M. Ciurana, F. Barcelo, J. Paradells, and E. Zola, "Performance evaluation of a TOA-based trilateration method to locate terminals in WLAN," *in Proc. of 1st IEEE International Symposium on Wireless Pervasive Computing*, January 2006.

[23] N. Patwari, A. O. Hero III, M. Perkins, N. S. Correal, R. J. O'Dea, "Relative location estimation in wireless sensor networks," *IEEE Transactions on Signal Processing*, vol. 51, no. 8, pp. 2137-2148, August 2003.

[24] N. Dragos, and B. Nath, "Ad hoc positioning system (APS) using AoA," *in Proc. of 22nd IEEE International Conference on Computer Communications (InfoCom)*, April 2003.

[25] A. Savvides, C. C. Han, and M. B. Srivastava, "Dynamic fine-grained localization in ad-hoc networks of sensors," *in Proc. of 7th ACM International Conference on Mobile Computing and Networking (MobiCom)*, July 2001.

[26] L. Cong and W. Zhuang, "Hybrid TDOA/AOA mobile user location for wideband CDMA cellular systems," *IEEE Transactions on Wireless Communications*, vol. 1, no. 3, pp. 439-447, July 2002.

[27] D. Niculescu, "Positioning in ad hoc sensor networks," *IEEE Networks*, vol. 18, no. 4, pp. 24-29, July 2004.

[28] K. Lorincz and M. Welsh, "Motetrack: a robust, decentralized approach to RF-based location tracking," *in Proc. of 1st International Workshop on Location- and Context-Awareness (LoCA)*, May 2005.

[29] P. Bahl and V. Padmanabhan, "RADAR: an in-building RF-based user location and tracking system," *in Proc. of 19th IEEE International Conference on Computer Communications (InfoCom)*, March 2000.

[30] G. Zhou, T. He, and J. A. Stankovic, "Impact of radio irregularity on wireless sensor networks," *in Proc. of 2nd ACM International Conference on Mobile Systems, Applications, and Services (MobiSys)*, June 2004.

[31] T. He, C. Huang, B. M. Blum, J. A. Stankovic, and T. Abdelzaher, "Range-free localization schemes in large-scale sensor networks," *in Proc. of 9th ACM International Conference on Mobile Computing and Networking (MobiCom)*, September 2003.

[32] R. Stoleru, T. He, J. A. Stankovic, and D. Luebke, "A high-accuracy, low-cost localization system for wireless sensor networks," *in Proc. of 3rd ACM International Conference on Embedded Networked Sensor Systems (SenSys)*, November 2005.

[33] K. R¨omer, "The lighthouse location system for smart dust," *in Proc. of 1st ACM International Conference on Mobile Systems, Applications, and Services (MobiSys)*, May 2003.

APPENDIX

A.

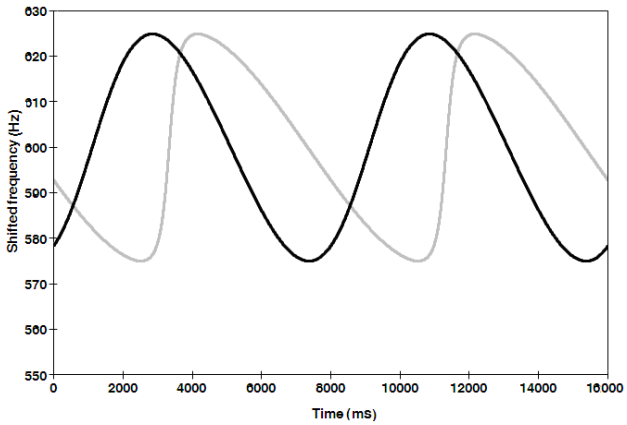

Figure 21. Non-approximated shifted frequency waveforms.

Figure 21 shows the simulation results for varying *r/d* ratios mentioned in Section 4. Two actual Doppler shifted frequency waveforms are constructed as follows:

$$\begin{cases} \Delta f_1(t) = 25\dfrac{\sin\left(\frac{360}{8000}\cdot t - 150\right)}{\sqrt{1+(0.8)^2-2\cdot(0.8)\cdot\cos\left(\frac{360}{8000}\cdot t - 150\right)}} \\ \Delta f_2(t) = 25\dfrac{\sin\left(\frac{360}{8000}\cdot t - 50\right)}{\sqrt{1+(0.2)^2-2\cdot(0.2)\cdot\cos\left(\frac{360}{8000}\cdot t - 50\right)}} \end{cases} \quad (17)$$

The two waveforms are constructed by substituting the following parameters into Equation (7) :

$$\begin{cases} \Delta f_1(t) : \omega rf/c = 25, \omega = \dfrac{360^\circ}{8000ms}, \dfrac{r}{d} = 0.8,\ \varphi - \alpha_1 = -150^\circ \\ \Delta f_2(t) : \omega rf/c = 25,\ \omega = \dfrac{360^\circ}{8000ms}, \dfrac{r}{d} = 0.2,\ \varphi - \alpha_2 = -50^\circ \end{cases} \quad (18)$$

The gray waveform in Figure 21 is the first shifted frequency waveform corresponding to Doppler shift $\Delta f_1(t)$, and the black waveform corresponds to $\Delta f_2(t)$. Note that the *y*-axis is the shifted frequency, which is the sum of the base frequency 600 Hz and the Doppler shift. Since *r/d* of the $\Delta f_1(t)$ is 0.8, which is far from zero, the waveform is quite different from a perfect sine wave.

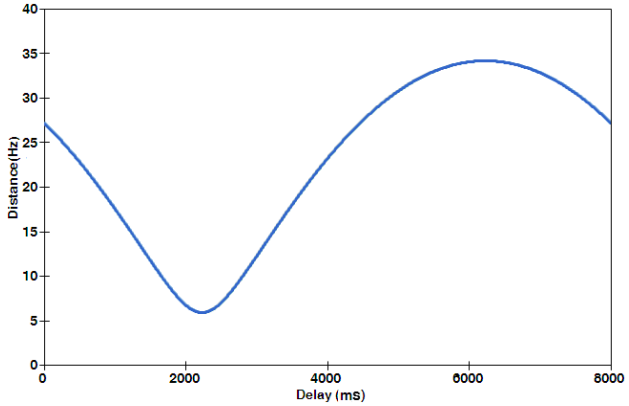

Figure 22. Distance between two signals in Figure 21 for different time delays.

The delay-and-compare method mentioned in subsection 3.3 is used to estimate the phase shift of the two waveforms. According to the simulation result in Figure 22, the minimum distance occurs when delay = 2,222 milliseconds. The corresponding minimum distance is 5.99 Hz. Since the period of both waveforms is 8,000 milliseconds, the estimated relative phase offset is (2,222/8,000)*360 = 100 degrees. The result equals the exact phase offset of the two approximated sinusoids. Further simulations with two *r/d* ratios varying from 0 to 1 reveal estimated phase offsets identical to the phase offsets used to generate the waveforms. This suggests that the approximation in the derivation of orientation angle calculation does not affect the location estimation error because the phase shift estimation method is not sensitive to the ratio of *r/d*.